Hydrothermal Growth of Hierarchical Ni_3S_2 and Co_3S_4 on a Reduced Graphene Oxide Hydrogel@Ni foam: A High-Energy-Density Aqueous Asymmetric Supercapacitor

Debasis Ghosh, Chapal Kumar Das*

Materials Science Centre, Indian Institute of Technology Kharagpur, India

E-mail: chapal12@yahoo.co.in

Materials used

$Co(NO_3)_2$, $Ni(NO_3)_2$, KOH and Na_2S, graphite powder, were bought from Loba chemie, India. Acetone, Ethanol were bought from E-Merc, India.

Characterizations

XRD analyses were carried out using Rigaku difractometer with a a PW1710 diffractometer, a Philips, Holland, instrument. Morphological characterizations were carried out in terms of FESEM (Carl Zeiss-SUPRATM 40), and TEM (TECNAI G2-20S-TWIN) analyses. Biologic sp-150 instrument was used for the electrochemical characterizations. Pore size distribution analysis was carried out using using Autosorb-1C instrument of Quantachrome Inc.

Equations used

For the three electrode cell, specific capacitance has been calculated from the GCD plot using the following equation

Specific capacitance $(C_s) = \dfrac{\int_{v1}^{v2} i\,(v)dv}{(v2-v1)\,vm}$ \qquad (1)

The neumerator indicates the area of the curve, V_2 and V_1 are the two potential, v is the scan rate and m is the mass of electroactive material.

Specific capacitance $\quad C_S = \frac{i \times t}{\Delta V \times m}$ (2)

Where, i/m is the mass normalized current, t is the discharge time and ΔV is the potential.

The energy density and power density can be calculated from the discharge plot using the following equation

Energy density (E) $= \frac{1}{2} C \times \Delta V^2$ (3)

Power density (P) = E/T (4)

Where, c is the specific capacitance obtained from GCD plots, V is the applied potential, T is the discharge time obtained from GCD plot.

For asymmetric supercapacitor a numerical value 4 has been multiplied to get the actual specific capacitance after considering 'm' as the mass of the total electroactive material comprising both anode and cathode .

Specific Capacitance from CV plot:

Specific capacitance (C_s) $= 4 \times \frac{\int_{v1}^{v2} i\,(v)dv}{(v2-v1)\,vm}$ (5)

Specific capacitance from GCD plot:

Specific capacitance $\quad C_S = 4 \times \frac{i \times t}{\Delta V \times m}$ (6)

The energy density was calculated from the GCD plot using the equation bellow:

Energy density $= \frac{1}{8} C * \Delta V^2$ (7)

The frequency dependent specific capacitance has been calculated from the Nyquist plot using the following equation

Specific capacitance (C_s) $= -\frac{1}{2} \times \pi \times f \times m \times Z_{img}$ (8)

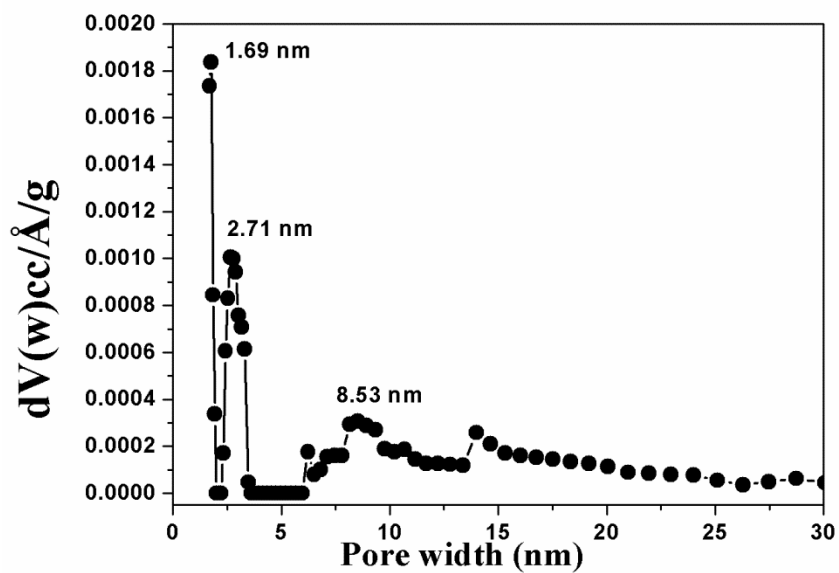Here f, m and Z_{img} are the frequency, mass of electroactive material and the imaginary impedance, respectively.

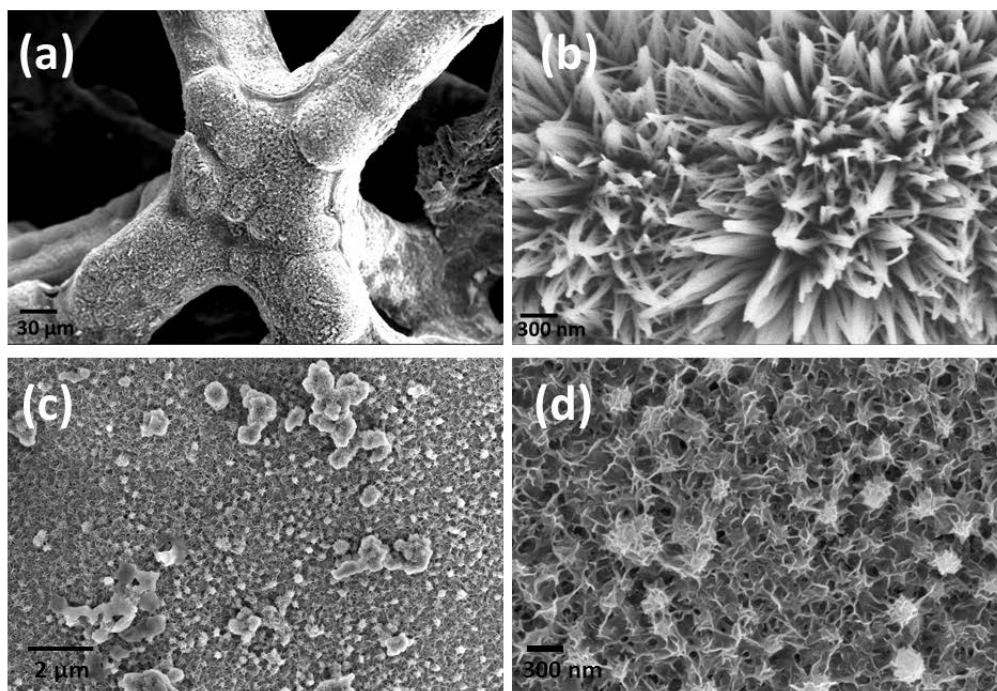**Figure S1.** Pore size distribution of rGO hydrogel after heat drying.

Figure S2. FESEM images of (a) Ni@Ni$_3$S$_2$ at low magnification; (b) Ni$_3$S$_2$ nanorods at high magnification; FESEM image of deposited Co$_3$S$_4$ film on Ni foam at low (c) and high magnification (d).

The FESEM image of the Ni@Ni$_3$S$_2$ (Figure S2 (b)) also indicates its nanorod morphology with uniform dimension, smooth surface and sharp end. The FESEM images of the Ni@Co$_3$S$_4$ indicates the porous film like architecture of the deposited Co$_3$S$_4$ over Ni foam.
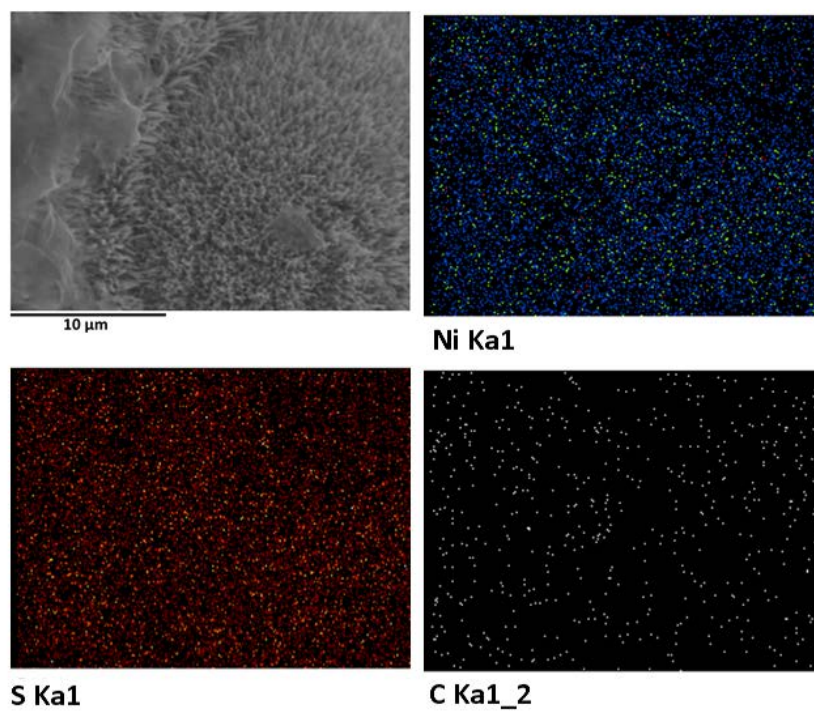

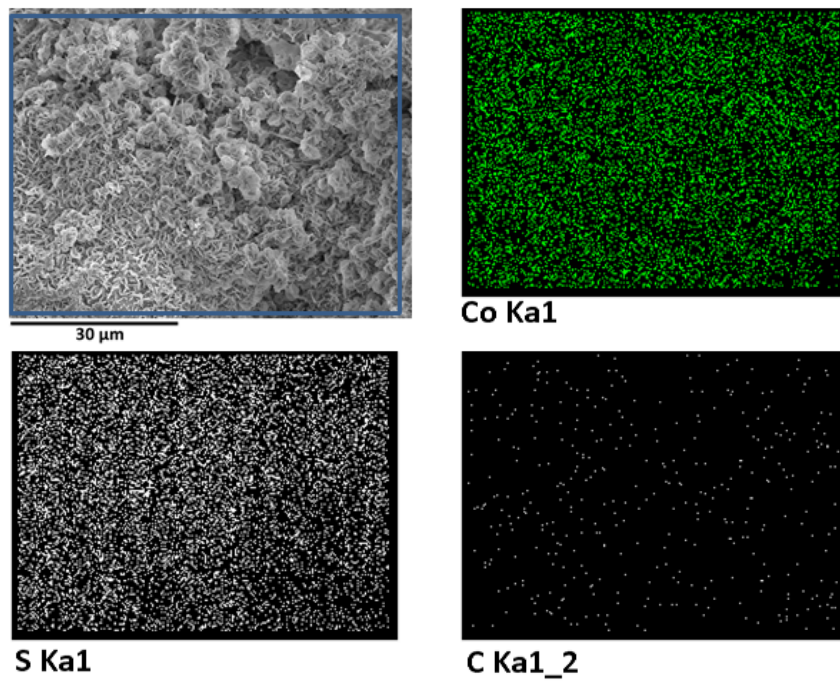**Figure S3**. Elemental mapping of Ni@rGO-Ni$_3$S$_2$

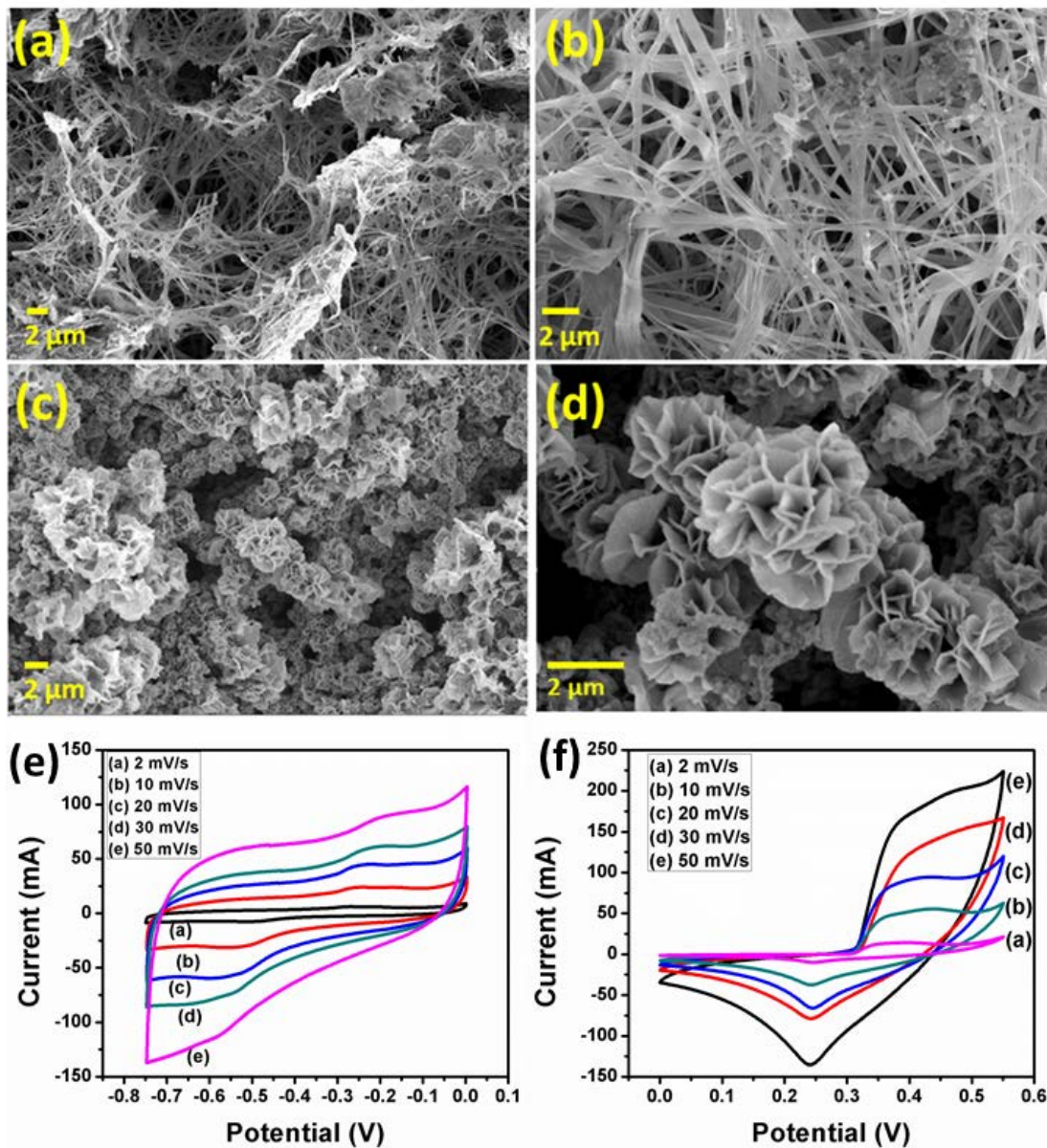**Figure S4**. Elemental mapping of Ni@rGO-Co$_3$S$_4$

Figure S5. FESEM images of Ni_3S_2 micro belt grown on Ni@rGO using high precursor concentration at various magnification (a, b); Co_3S_4 micro flower at different magnification (c, d); CV plots of the as grown Ni_3S_2 microbelt grown over Ni@rGO (e) and Co_3S_4 microflower grown over Ni@rGO (f) at different scan rates of 2, 10, 20, 30, and 50 mV/s.

The Ni_3S_2 and Co_3S_4 were also grown on the Ni@rGO substrate using the same amount of precursor of 10 ml 0.1 M Na_2S with 10 ml 0.1 M $Ni(NO_3)_2$ and 10 ml 0.1 M $Co(NO_3)_2$,

respectively and hydrothermally treated for 15h. Unlike the Ni@rGO-Ni$_3$S$_2$, the FESEM image of as grown Ni$_3$S$_2$ over Ni@rGO (Figure S4 a, b) after 15h of hydrothermal treatment indicates its microbelt morphology with smooth surface and 1.5-2μm width. The increase in hydrothermal reaction time results in the enlargement of the nanorod Ni$_3$S$_2$ and microbelt morphology was achieved. In case of the Co$_3$S$_4$, the enhanced hydrothermal reaction time results in further growth of the cross linked nanosheet network and at the end microflower architecture was achieved. The deposition of the active material on the Ni@rGO substrate was simply increased by increasing the hydrothermal reaction time. An increase in reaction time from 6h to 15 h resulted in the active material mass of 3.9 mg (from 2.8 mg) and 3.75 mg (from 2.7 mg), respectively for the Ni@rGO-Ni$_3$S$_2$ and Ni@rGO-Co$_3$S$_4$. This increases the thickness of the active material over the current collector, and decreases the effective use of the entire active material due to less transportation of charge. The CV plots of the as grown Ni$_3$S$_2$ microbelt and Co$_3$S$_4$ microflower grown over Ni@rGO are shown in Figure S5 (e) and S5 (f), respectively at different scan rates of 2, 10, 20, 30, and 50 mV/s. The maximum specific capacitances of 1076 F/g and 1426 F/g were achieved at 2 mV/ s scan rate.